Table 1-1 Comparison between vacuum microelectronics and solid-state electronics.

Items	Solid State Microelectronics	Vacuum Microelectronics
Current Density	$10^4 – 10^5$ (A/cm^2)	similar
Turn-on Voltage	0.1 – 0.7 V	5 – 300 V
Structure	solid/solid interface	solid/vacuum interface
Electron Transport	in solid	in vacuum
Electron Velocity	3×10^7 (cm/sec)	above 3×10^8(cm/sec)
Flicker Noise	due to interface	due to emission
Thermal & Short Noise	comparable	comparable
Electron Energy	< 0.3 eV	a few to 1000 eV
Cut-off Frequency	< 20 GHz (Si) & 100 GHz (GaAs)	< 100 – 1000 GHz
Power	small – medium	medium – large
Radiation Hardness	poor	excellent
Temperature Effect	-30 – 50 °C	< 500 °C
Fabrication & Materials	well established (Si) & fairly well (GaAs)	not well established

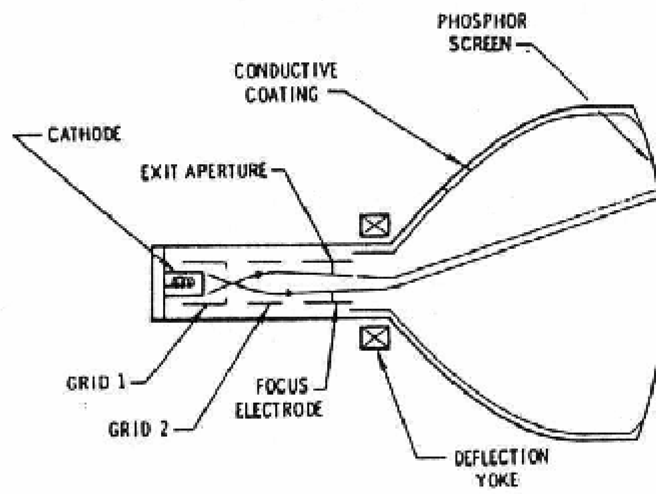

(a)

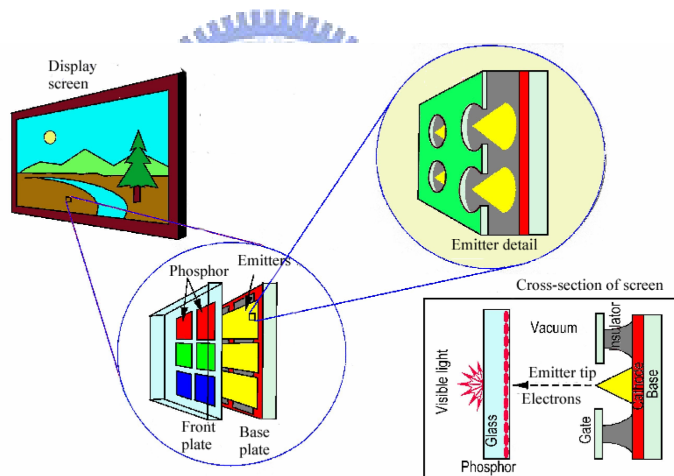

(b)

Fig. 1-1 The schematic diagram of (a) conventional CRT, (b) FED.

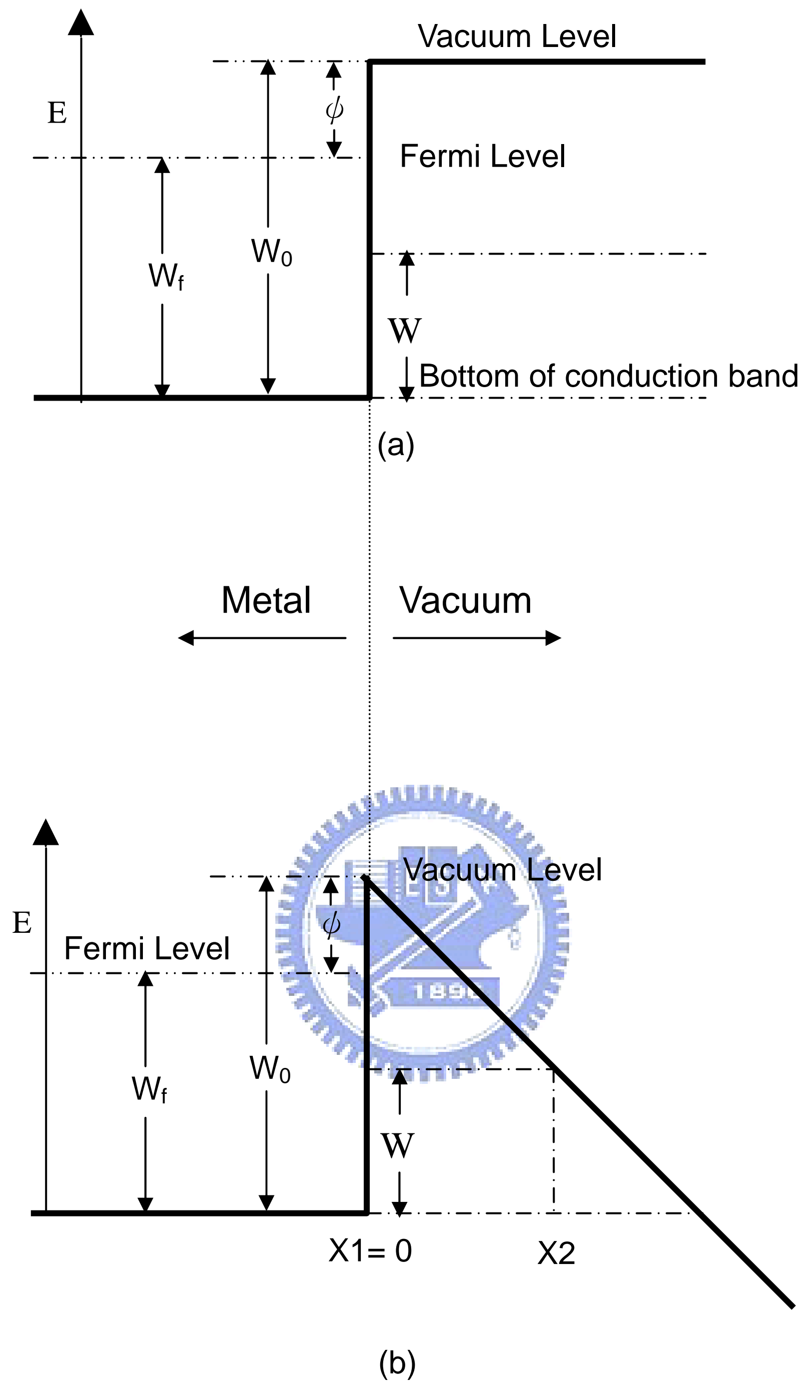

Fig. 1-2 Energy diagrams of vacuum-metal boundary:

(c) without external electric field;

(d) with an external electric field.

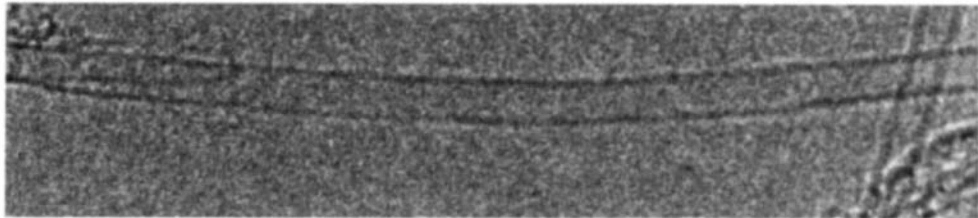

(a)

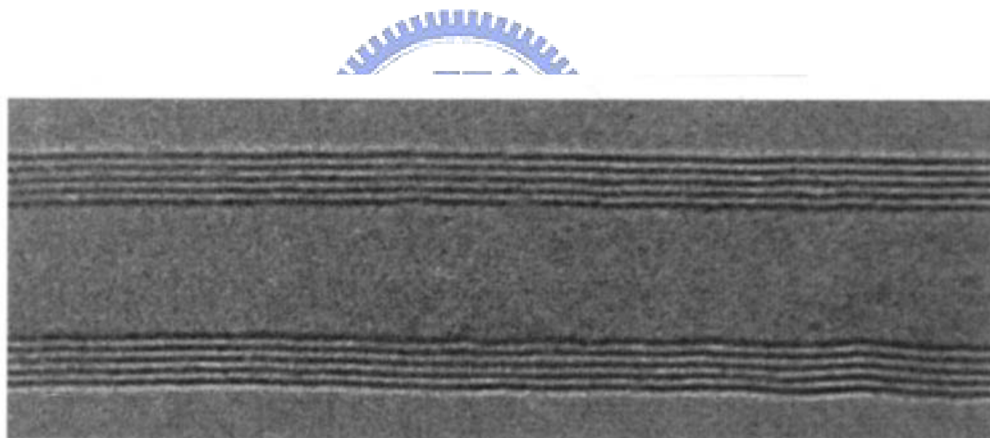

(b)

Fig. 1-3 High-resolution transmission electron microscopy images of (a) single-walled nanotubes (SWNTs) and (b) multiwalled nanotubes (MWNTs). Every layer in the image (fringe) corresponds to the edges of each cylinder in the nanotube assembly.

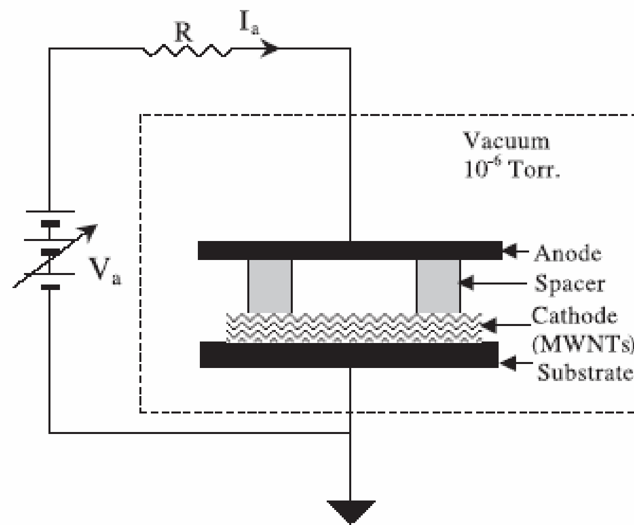

(a)

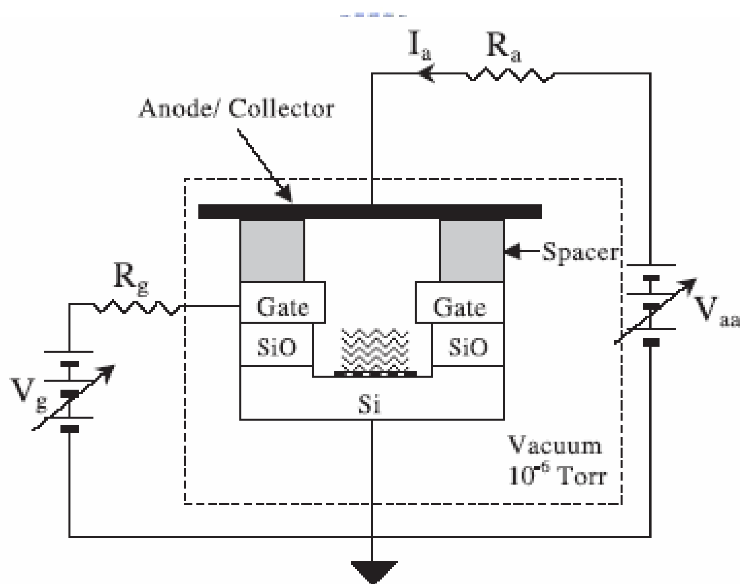

(b)

Fig. 1-4 Schematic diagrams of the emission testing circuits for (a) MWNTs vacuum diode, and (b) the self-aligned MWNTs vacuum triode. (Ref. Diamond & Related Materials 13 (2004) 2105– 2112)

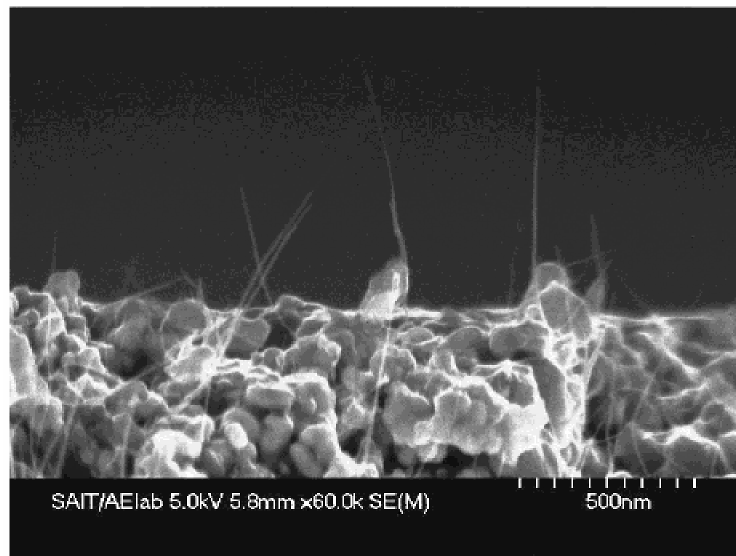

(a)

(b)

Fig. 1-5 (a) SEM image of CNT cathode from Samsung's FED.

(b) Demonstration of a 4.5-inch FED from Samsung. The emitting image of fully sealed SWNT-FED at color mode with red, green, and blue phosphor columns.

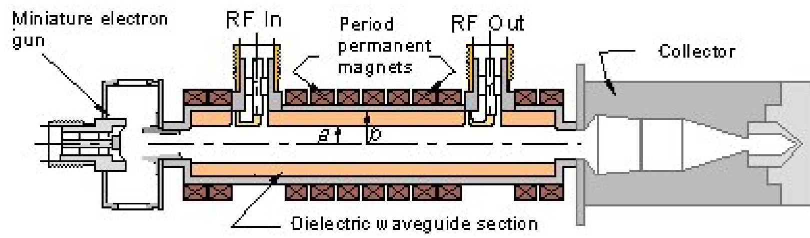

(a)

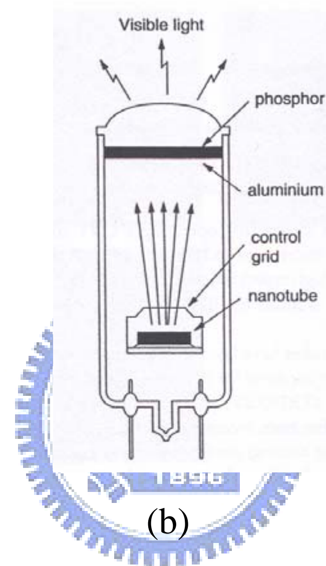

(b)

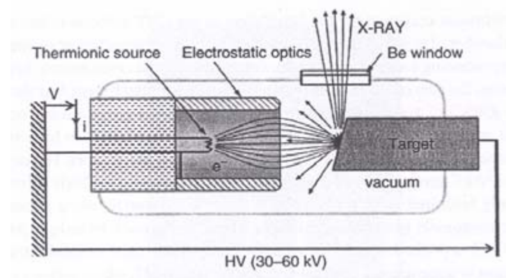

(c)

Fig. 1-6 All device have been based on field emitter array (FEA) cathodes that were used as : (a) TWT, (b) LED, (c) X-ray tube
(Ref. Carbon Nanotubes Science And Applications, M. Meyyappan page 205)
)

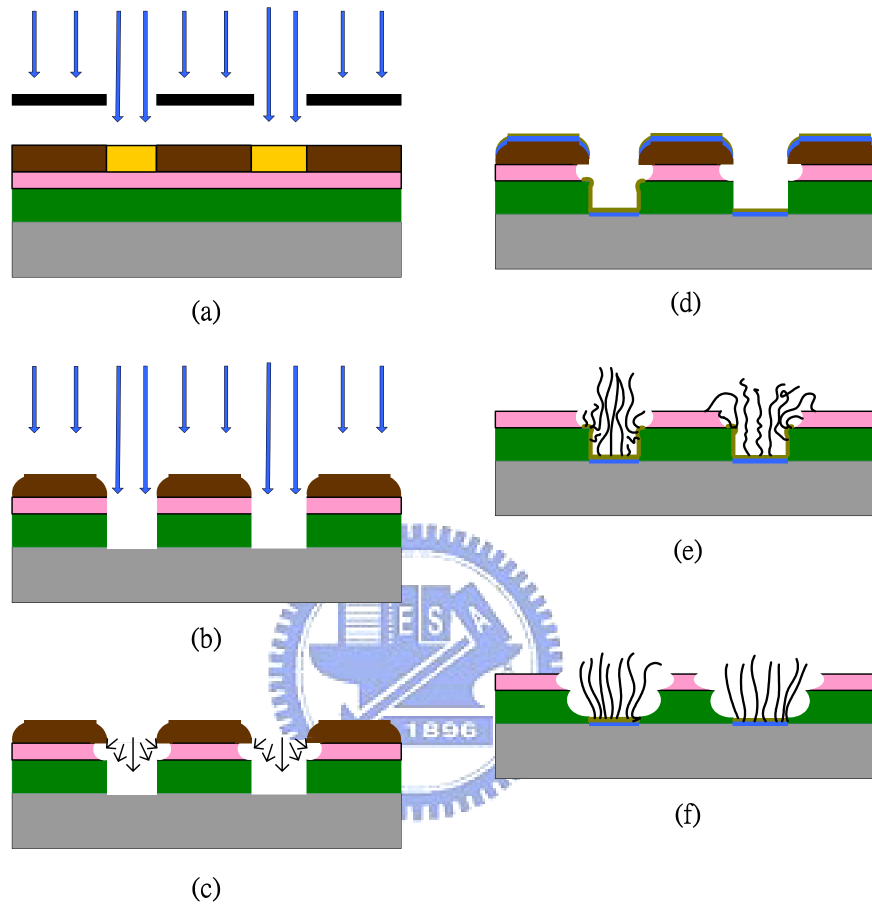

Fig. 1-7 (a)~(d) Flow chart of conventional lateral device, two drawbacks of this structure: (e) The short circuit between the emitters to electrode, (f) The electrode is eched back to void short circuit and the electrical characteristic is worse.

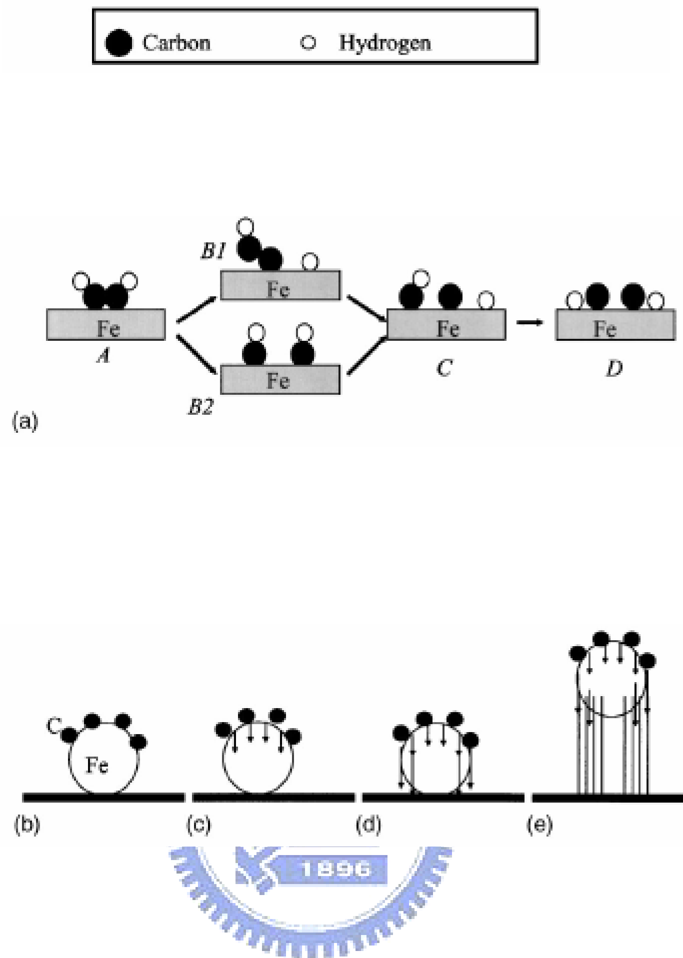

Fig. 2-1. (a) Sequences of dissociative adsorption of C2H2 on Fe surface. The (b) decomposed carbon atoms (c) diffused into the Fe nanoparticle until (d) supersaturation and (e) segregate as nanotubes. Ref. Appl. Phys. Lett. 85 (2004) 3265

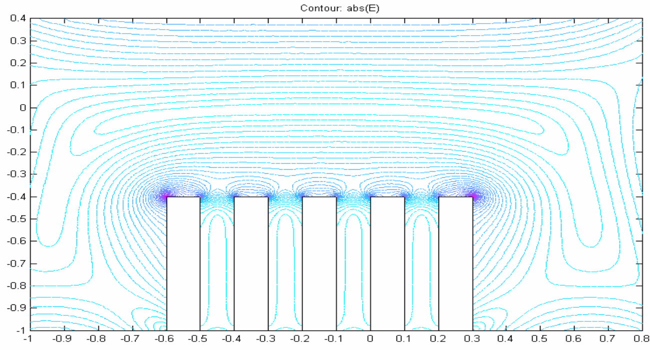

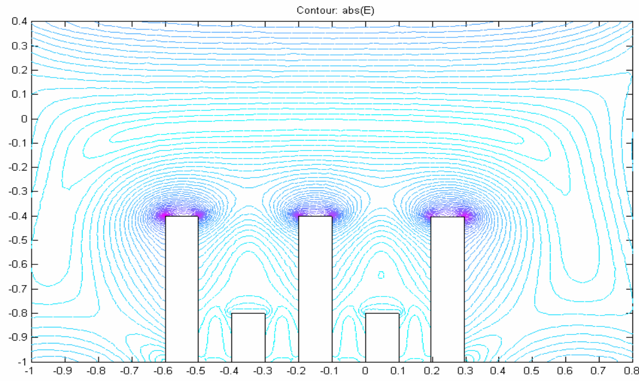

Fig. 2-2 Simulation of screening effect.

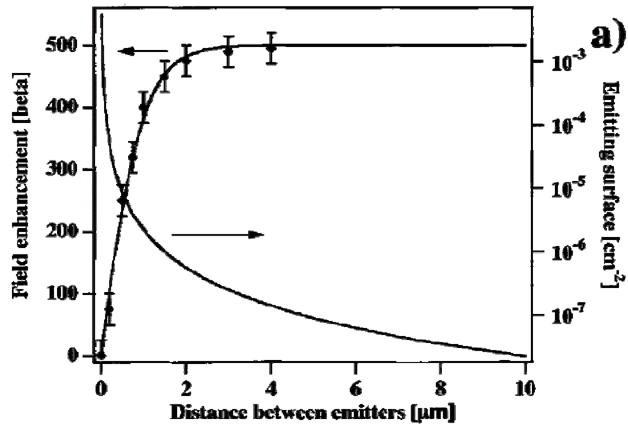

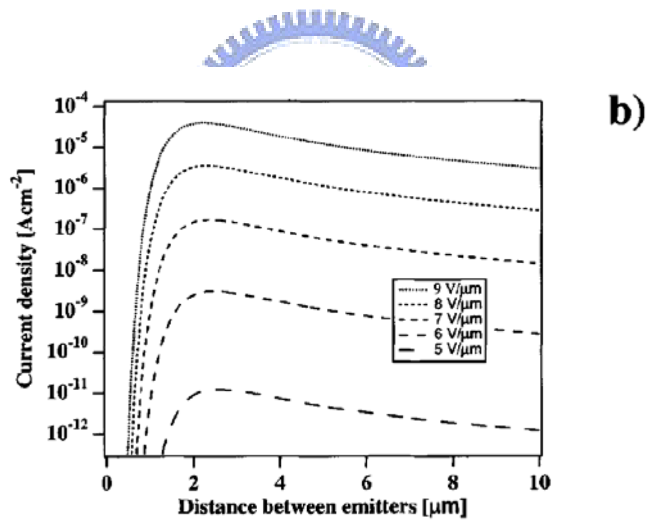

Fig. 2-3 (a) Relation between the field enhancement factor and the spacing between the tips (a square array of tips 4 nm in diameter and 1 μm in length), as well as the decrease of the total emitting surface due to decreasing tip density with increasing intertip spacing.

(b) The emission current density was calculated by the F-N equation at different applied fields. (J. Vac. Sci. & Technol. B, Vol. 18(2), p. 665, 2000)

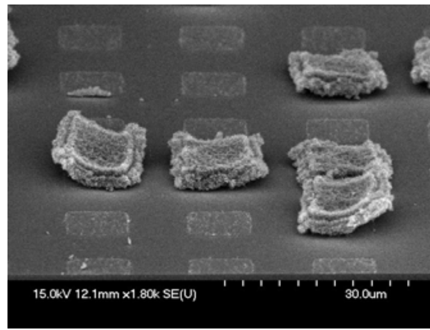

(a)

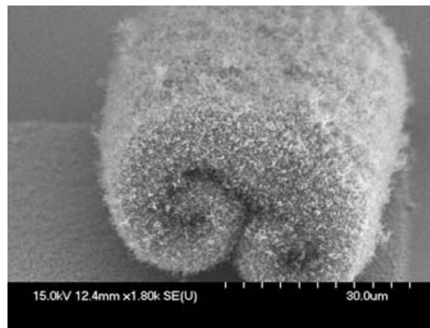

(b)

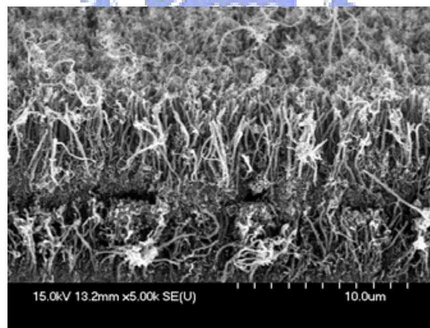

(c)

Fig. 2-4 SEM micrographs of CNTs with poor adhesion (a) The catalyst falls off from the substrate (b) The catalyst rolls up from the substrate (c) Double Layer of CNTs: The catalyst layer is too thick, the excess metal-unused as catalyst at the top of the tower

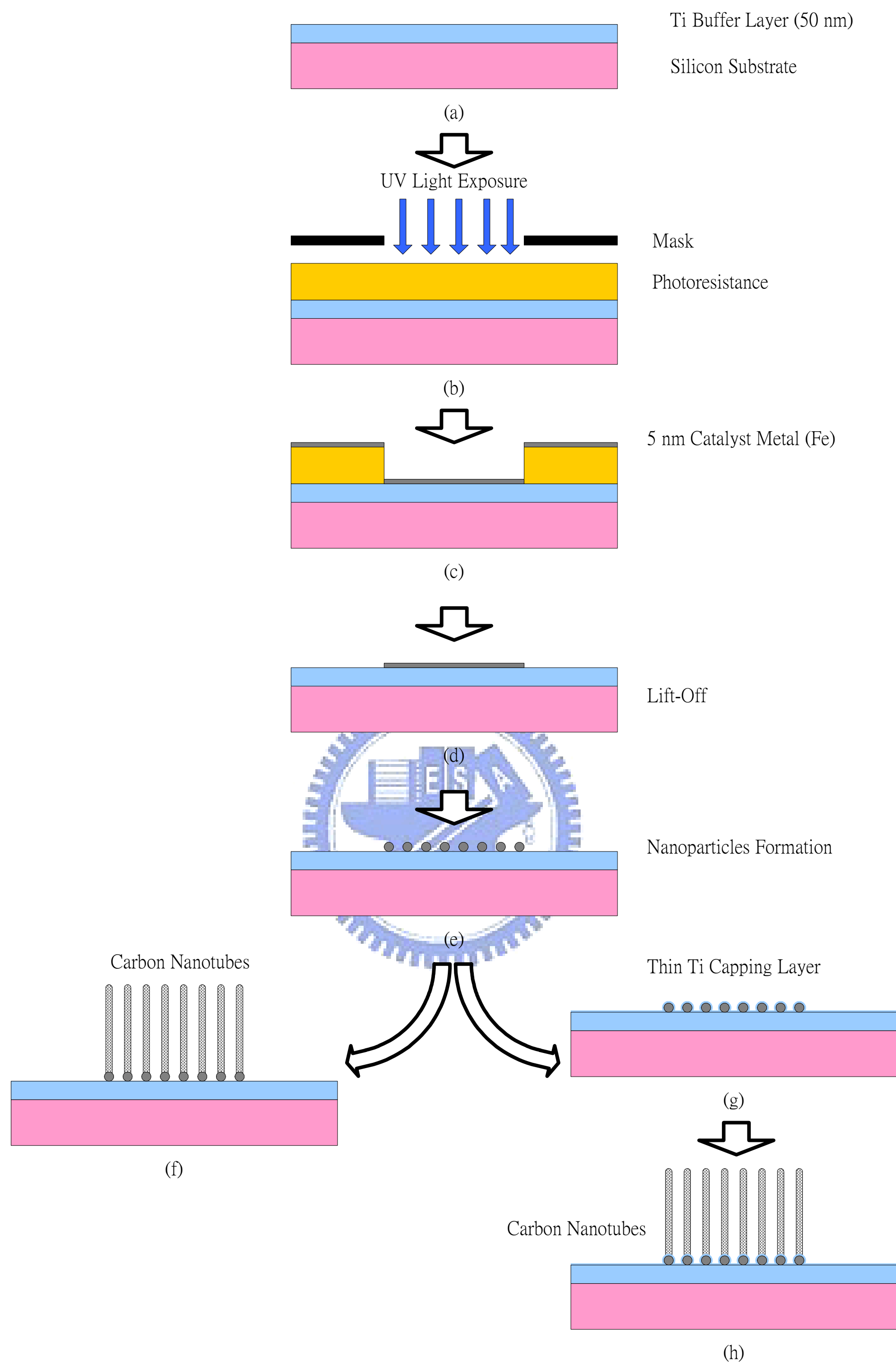

Fig. 2-5 Experimental procedures of CNTs synthesize by capping layer

(a)

(b)

(c)

Fig. 2-6 Photographs of material analysis instrument (a)SEM, (b)TEM, (c)Raman Spectrum

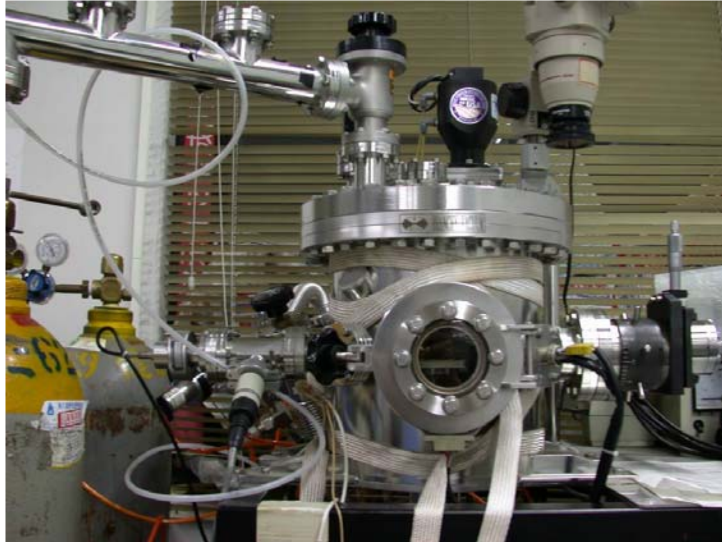

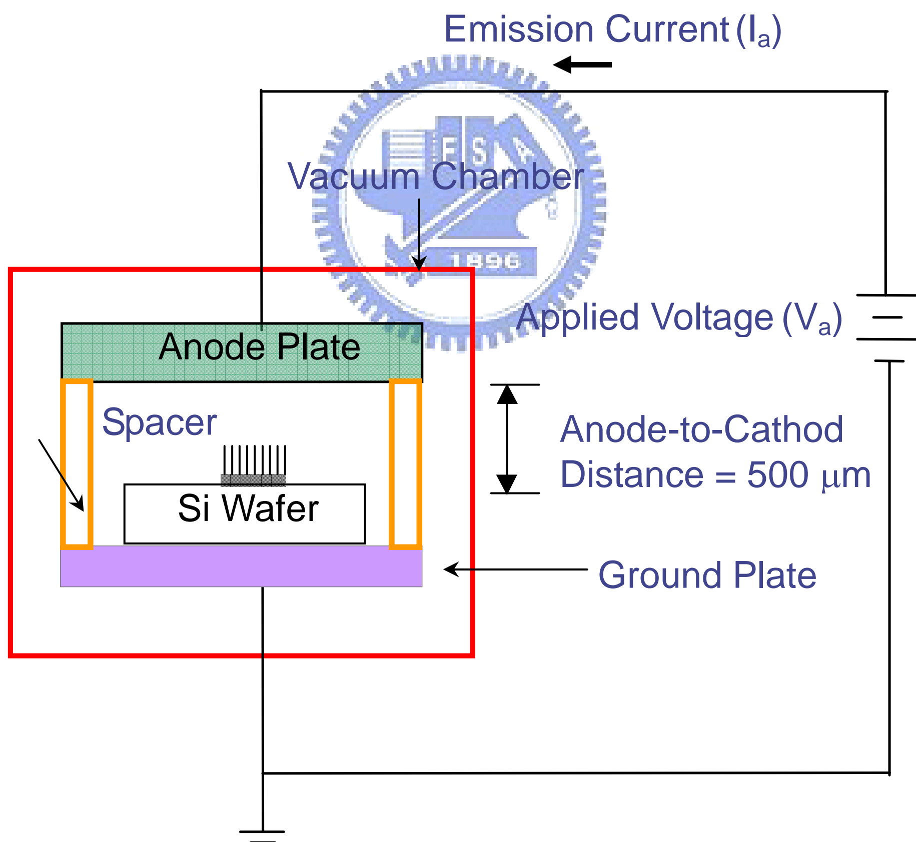

Fig. 2-7 High vacuum measurement system.

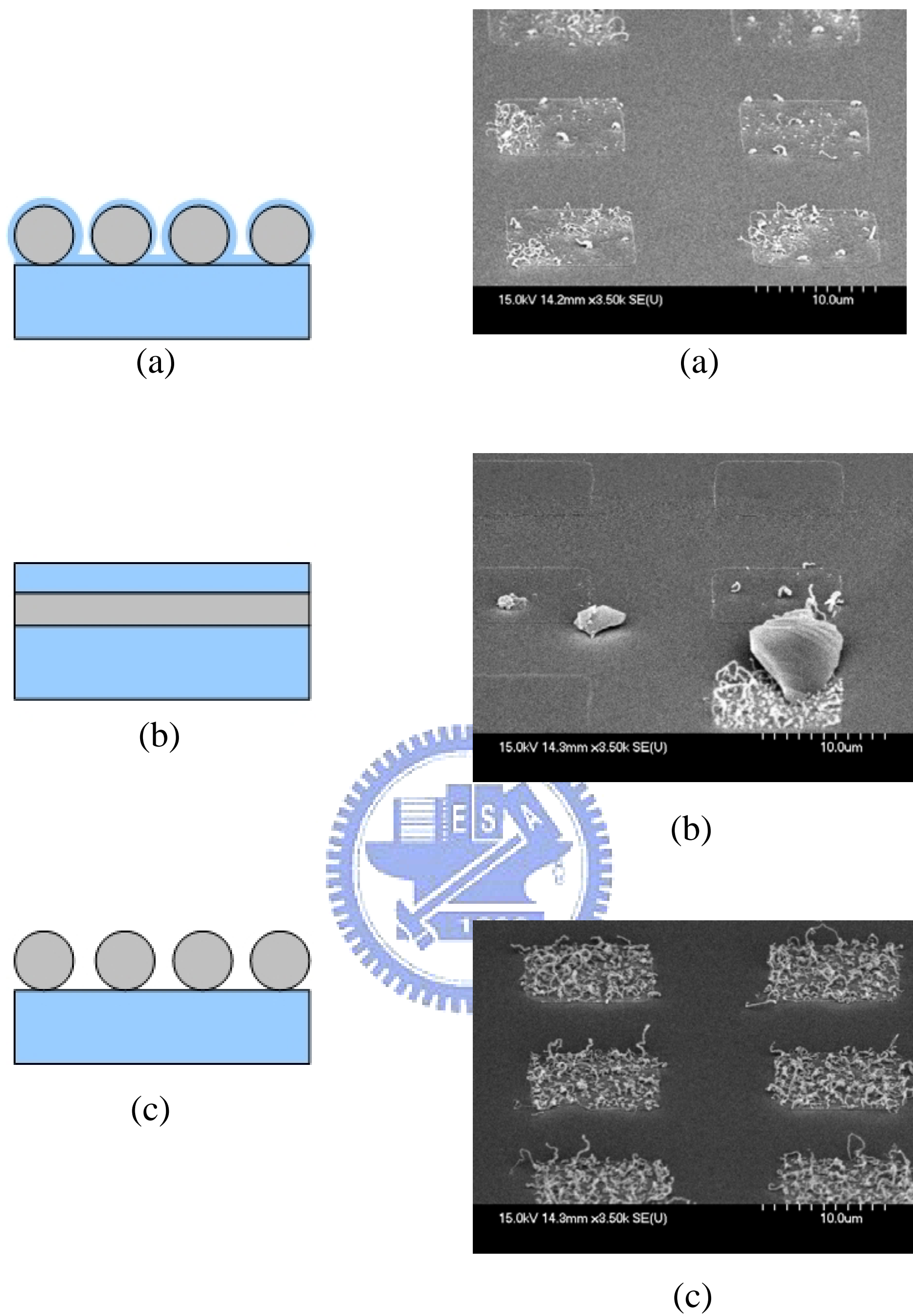

Fig. 2-8 SEM micrographs of (a) capping Ti 100A with Fe pretreatment, (b) capping Ti 100A without Fe pretreatment (c) without capping metal

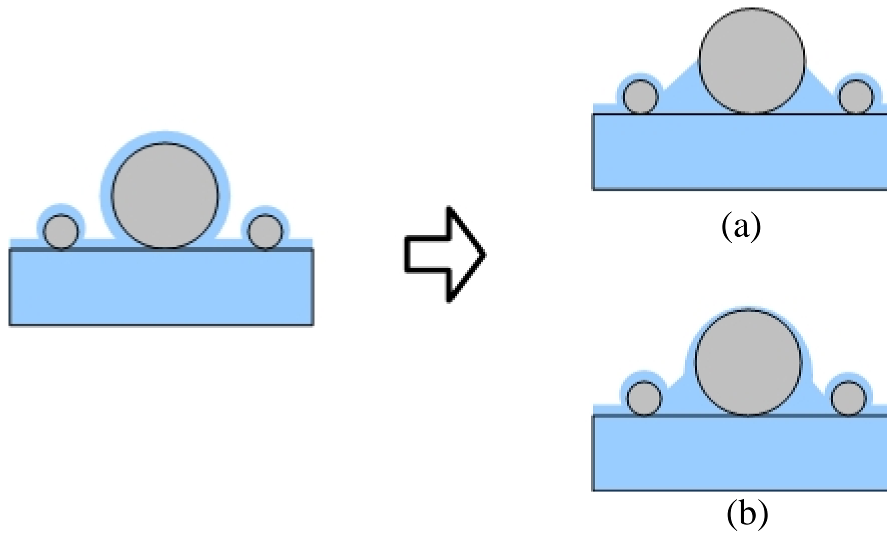

Fig. 2-9 Illustrate of two synthesis mechanism by Ti atoms gathering and (a) expose Fe catalyst (b) thin enough for carbon diffusion.

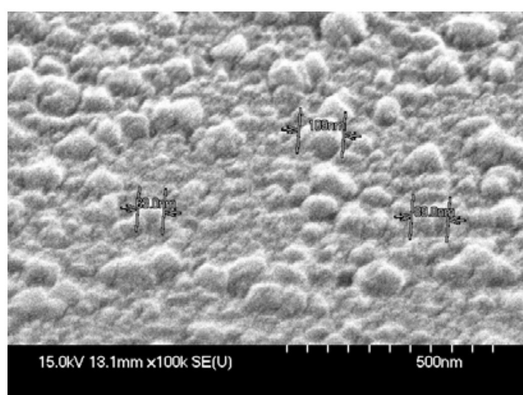

(a) Fe 50A

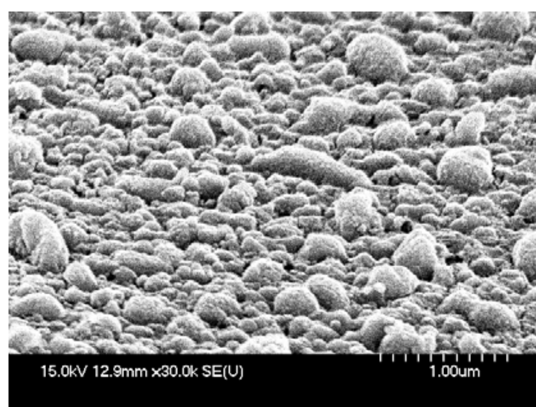

(b) Fe 100A

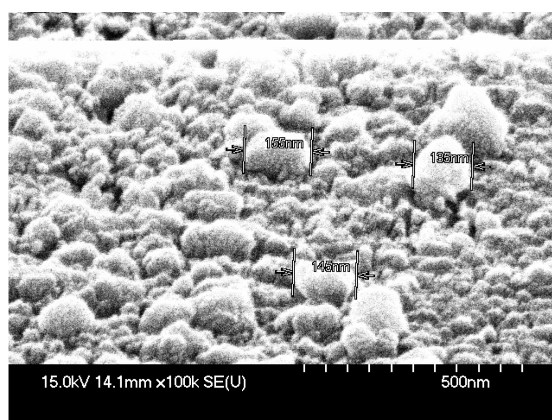

(c) Fe 500A

Fig. 2-10 SEM micrographs of catalyst pretreatment with different thickness in H_2 500sccm at 700℃ and the nanopartical is about (a) 80nm, (b) 100nm and (c) 150nm

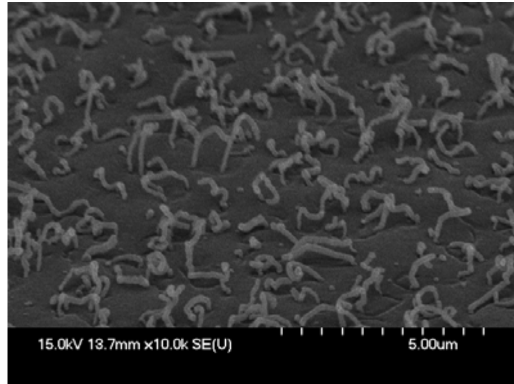

(a) Fe 50A

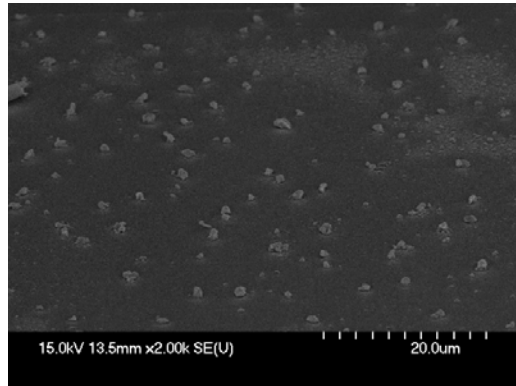

(b) Fe 100A

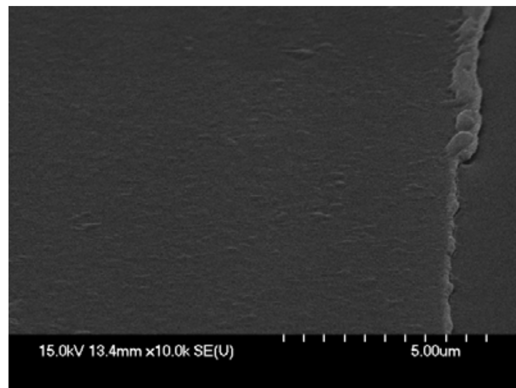

(c) Fe 500A

Fig. 2-11 SEM micrographs of CNTs synthesize at different catalyst thickness with capping Ti 100A

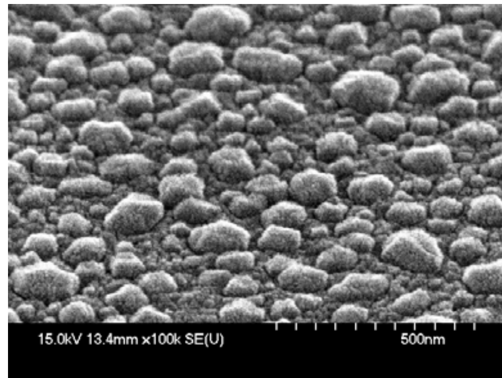

(a) pretreatment 5mins

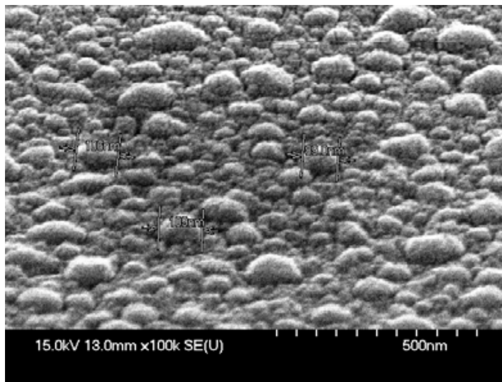

(b) pretreatment 15mins

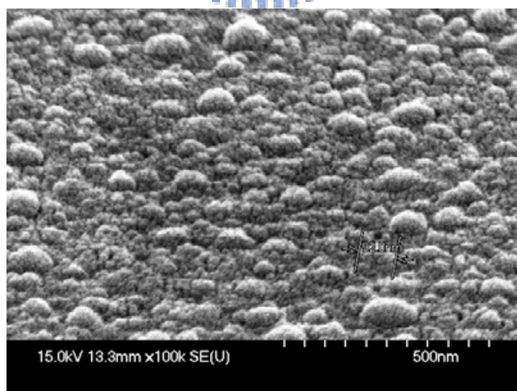

(c) pretreatment 30mins

Fig. 2-12 SEM micrographs of catalyst with different pretreatment time (a) 5mins, (b)15mins and (c) 30mins in H_2 500sccm at 700℃

Figure 2.13: A liquid droplet in equilibrium with a horizontal surface surrounded by a gas. The wetting angle θ between the horizontal layer and the droplet interface defines the wettability of the liquid.

Metal	Melting point
Ti	1668 ˚C
Al	660 ˚C
Mo	2623˚C
Fe	1583 ˚C

Table 2-1 The melting point of metal use for capping layer

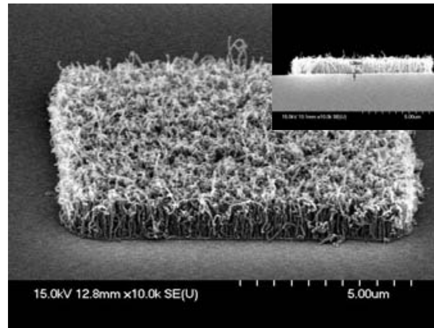

(a)

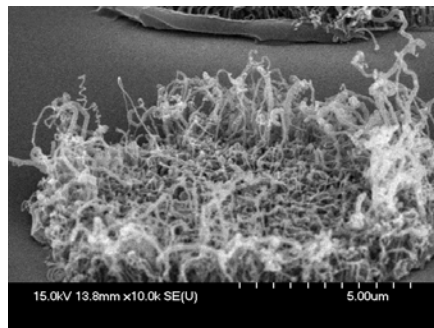

(b)

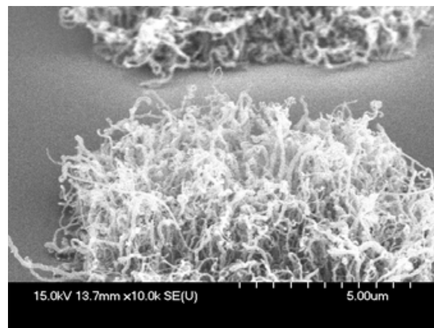

(c)

Fig. 2-14 SEM micrographs of CNTs with different pretreatment time (a) 5mins, (b)15mins and (c) 30mins in H_2 500sccm at 700℃

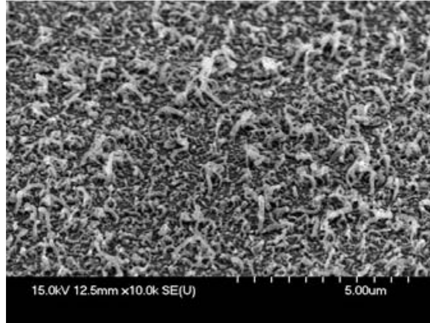

(a) Capping Ti 50A

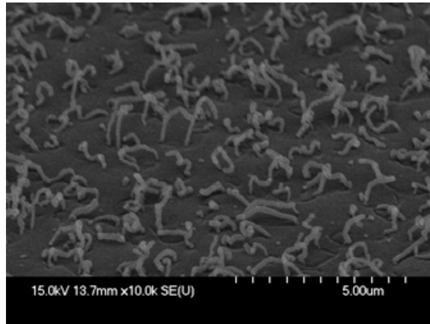

(b) Capping Ti 100A

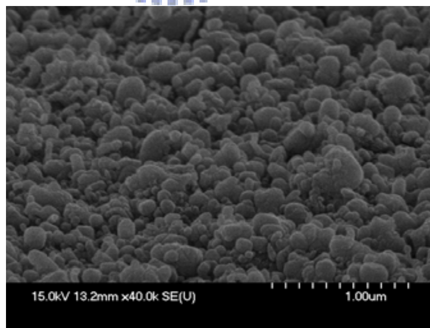

(c) Capping Ti 500A

Fig. 2-15 SEM micrographs of (a) capping Ti 50A, (b) capping Ti 100A and (c) capping Ti 500A

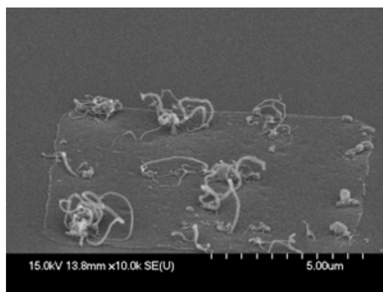

(a) Mo

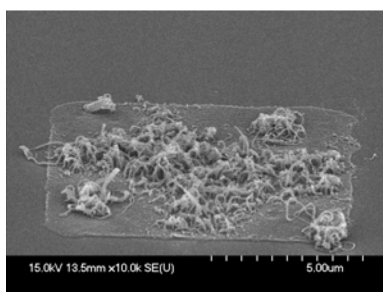

(b) Ti

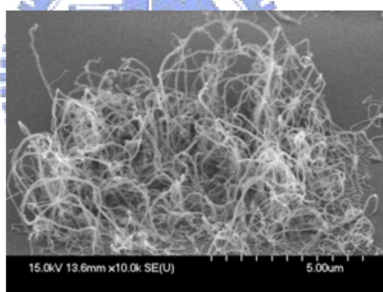

(c) Al

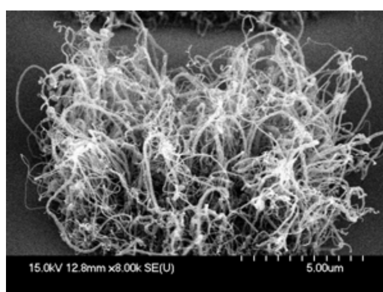

(d) without capping metal

Fig. 2-16 SEM micrographs of (a) capping Mo, (b) capping Ti, (c) capping Al and (d) without capping metal. All capping metal is deposited after catalyst

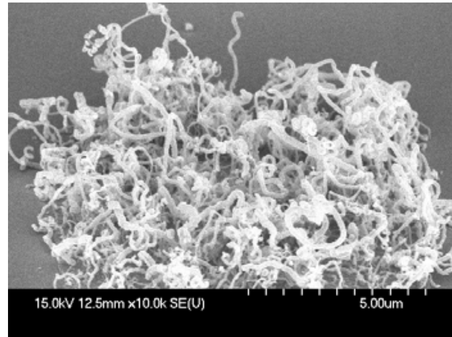

(a)

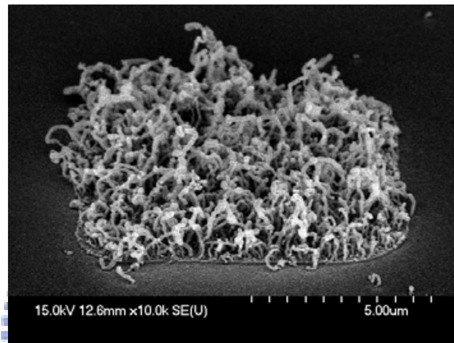

1896
(b)

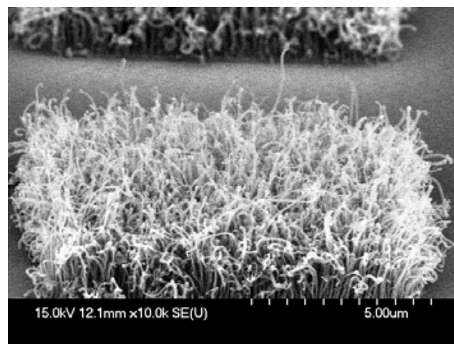

(c)

Fig. 2-17 SEM micrographs of (a) capping Ti 50A after Fe pretreatment, (b) capping Ti 50A without Fe pretreatment, (c) without capping metal.

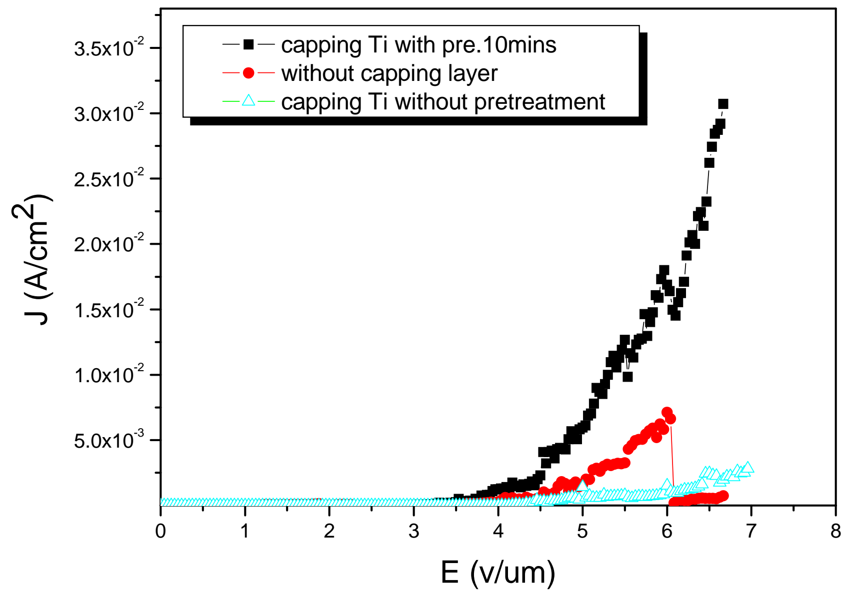

(a)

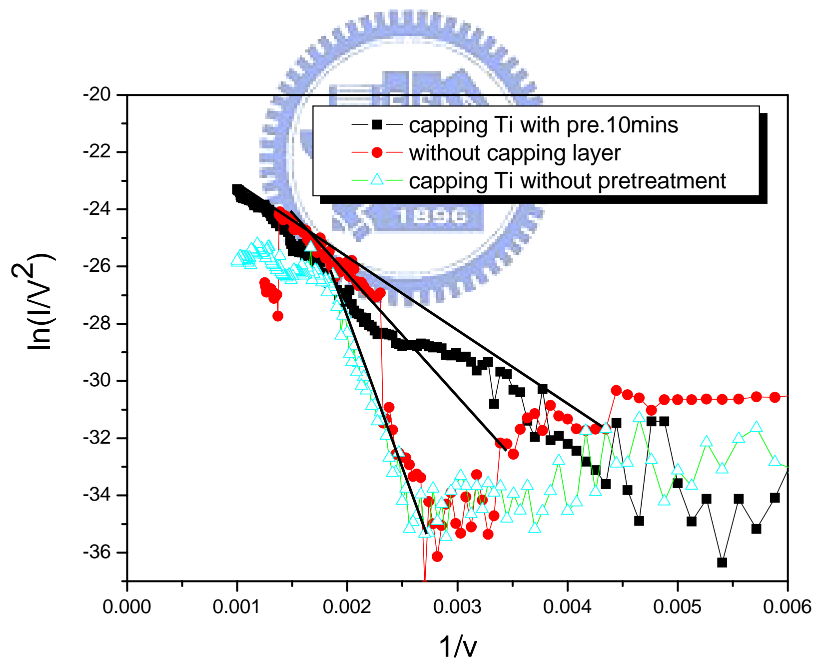

(b)

Fig. 2-18 (a) Characteristics of emission current density (J) versus applied electric field (E) for the CNTs with (i) capping Ti after pretreatment, (ii) capping Ti without pretreatment (iii) without capping layer, (b) the corresponding F-N plots.

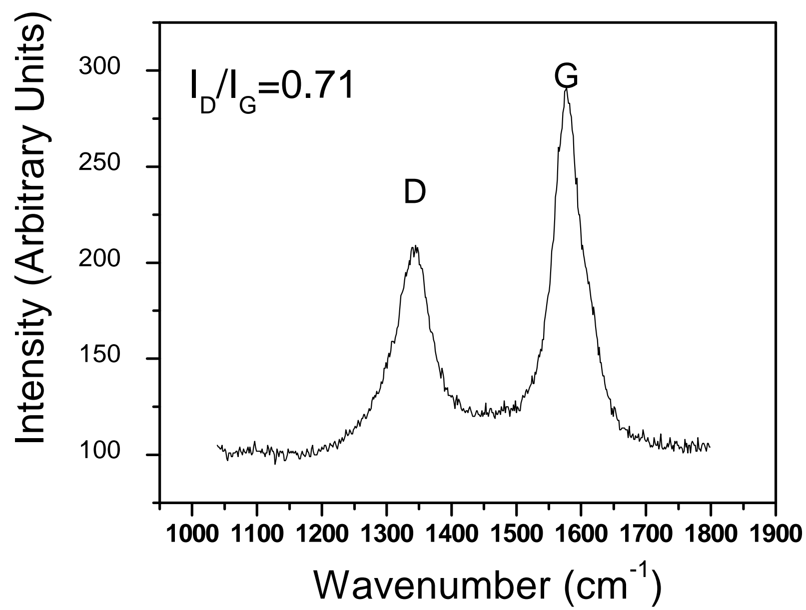

(a)

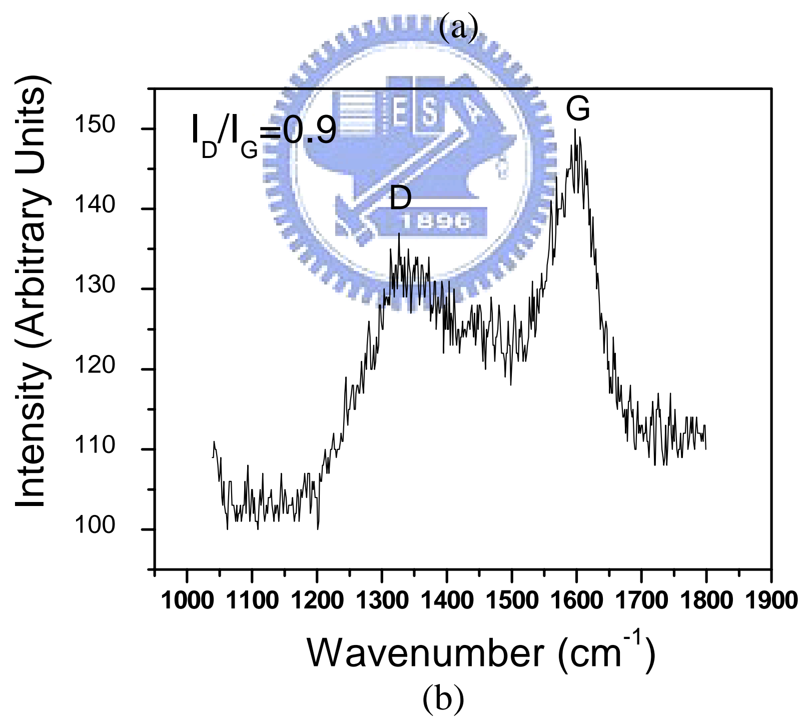

(b)

Fig. 2-19 Raman spectra of the CNTs grown at 700℃ (a) without capping layer, (b) with Ti 50A capping layer after catalyst pretreatment.

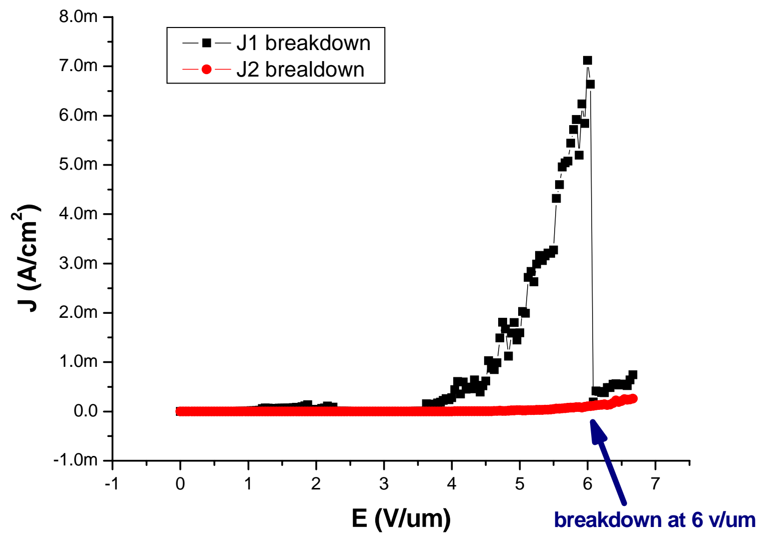

(a)

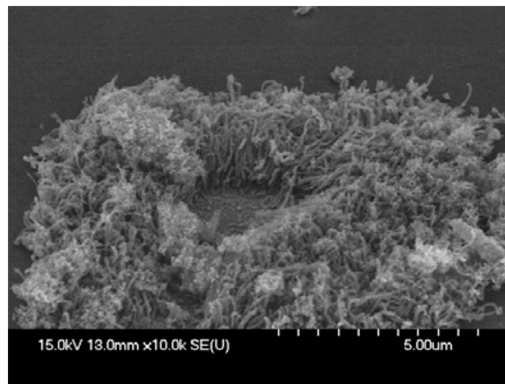

(b)

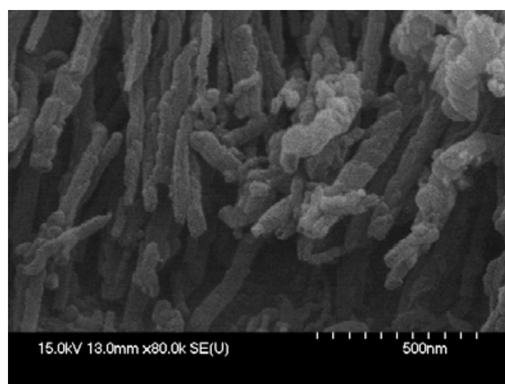

(c)

Fig. 2-20 (a) Characteristics of emission current density (J) versus applied electric field (E) for the CNTs before and after breakdown, (b)SEM micrographs of CNTs breakdown at 6.5v/um, (c) enlarge view (80K) at the bottom of CNT.

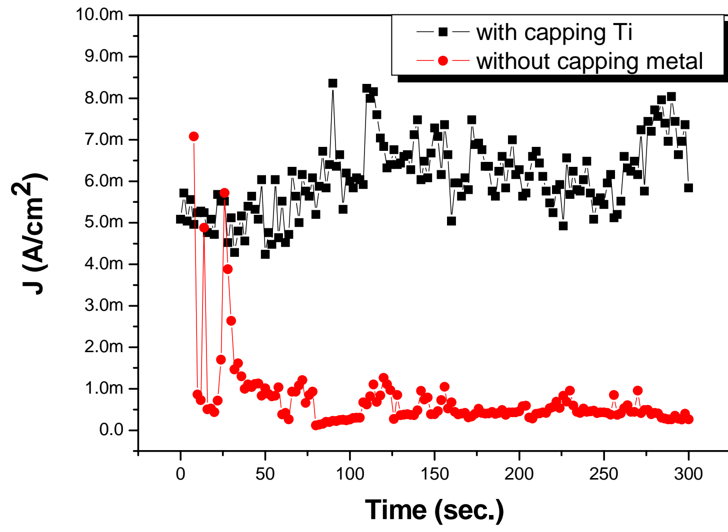

(a)

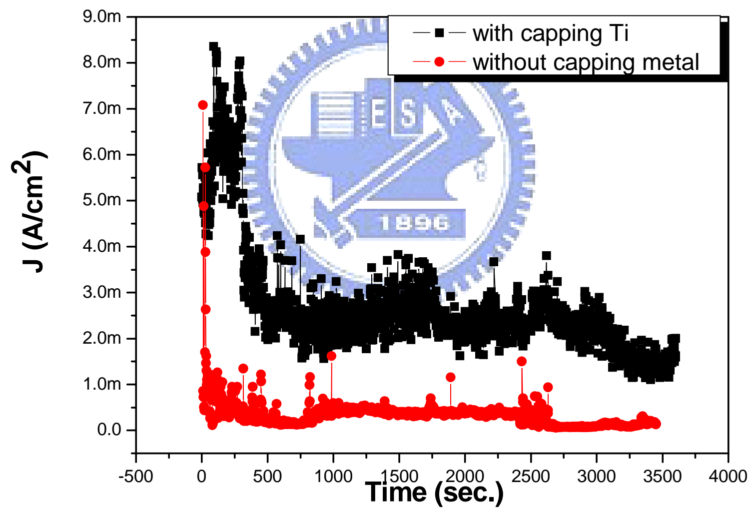

(b)

Fig. 2-21 Characteristics of stress for the CNTs at: (a) 10v/um for 5minutes, (b) 10v/um for 1hr.

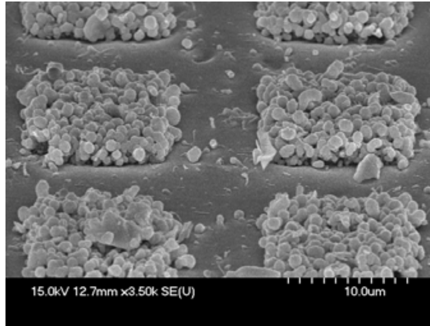

(a)

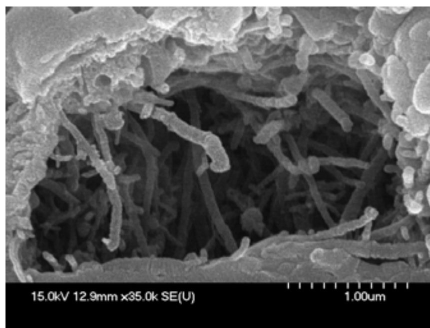

(b)

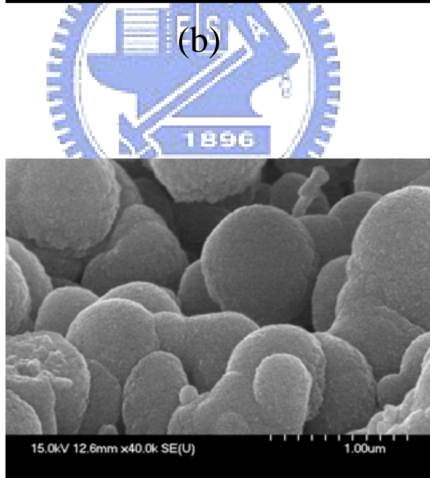

(c)

Fig. 2-22 SEM micrographs of the stress of CNTs at high voltage 1000v for 1hr and the nanotubes melt down by joule heating.

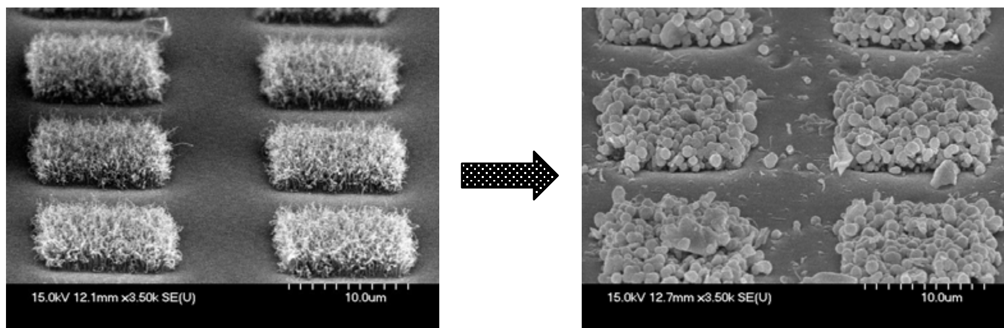

(a)

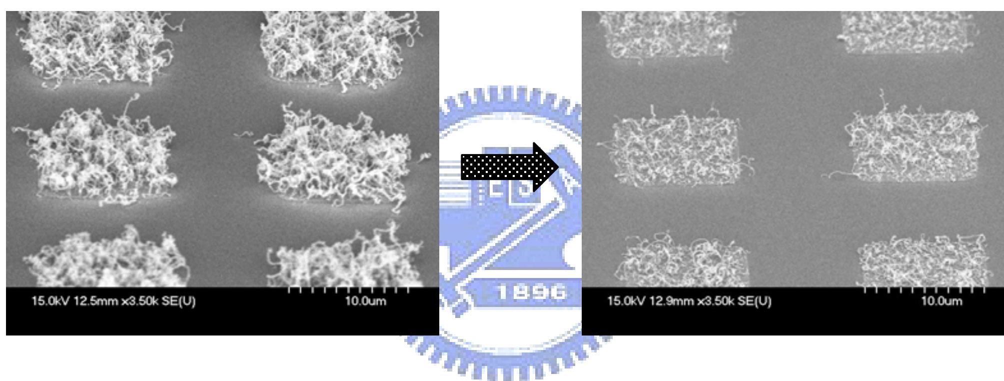

(b)

Fig. 2-23 SEM micrographs of the CNTs after and before stress
(a) with capping layer, (b) and without capping layer.

(a)

(b)

Fig. 2-24 Photographs of the light emitted by the phosphor screen for a rectangular aligned CNTs array (a) with capping layer, (b) without capping layer

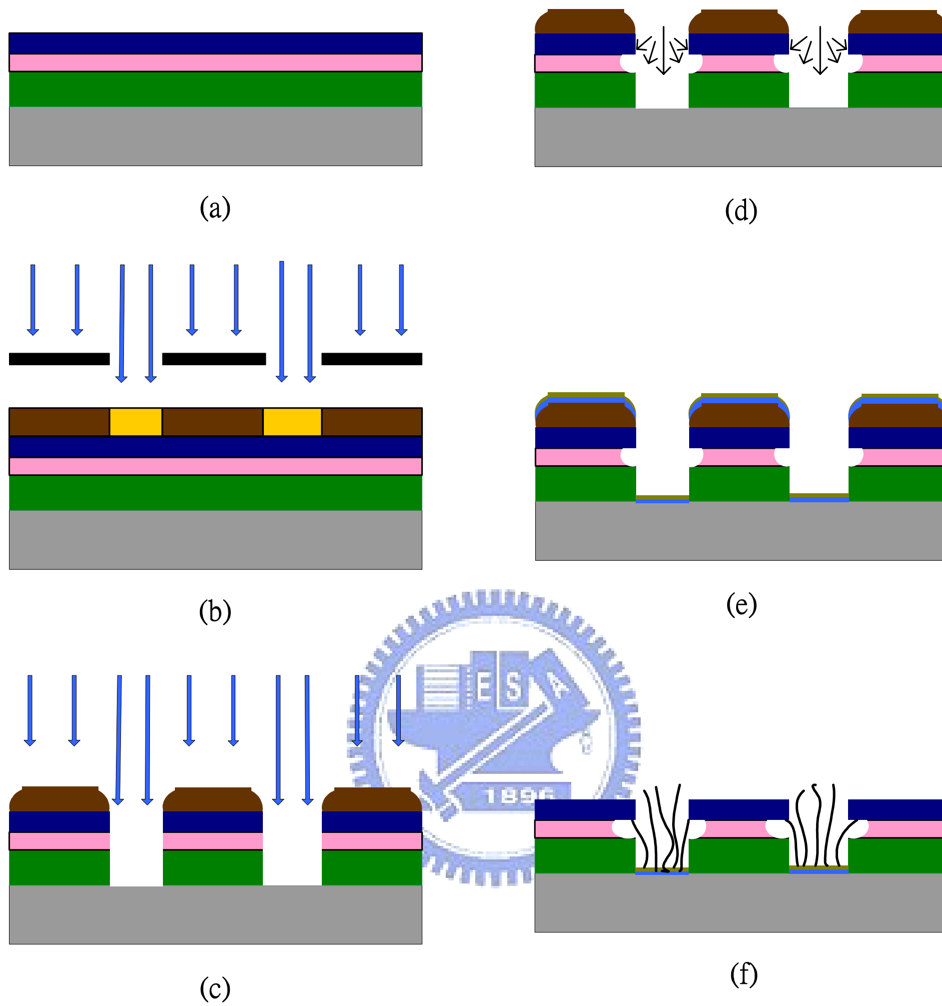

Fig. 3-1 Fabrication procedure of the carbon nanotubes nitride-insulated electrode structure field emission device.

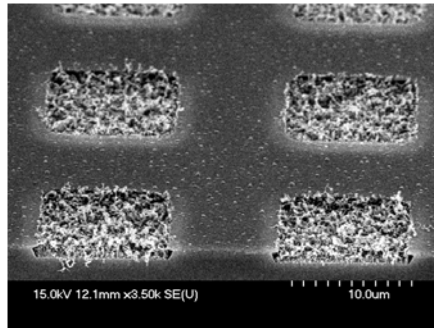

(a)

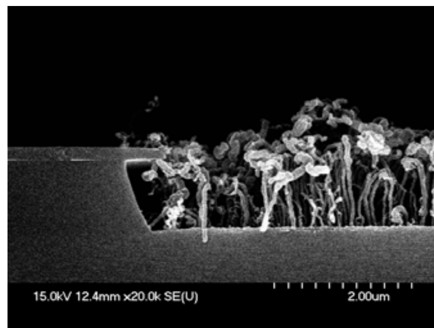

(b)

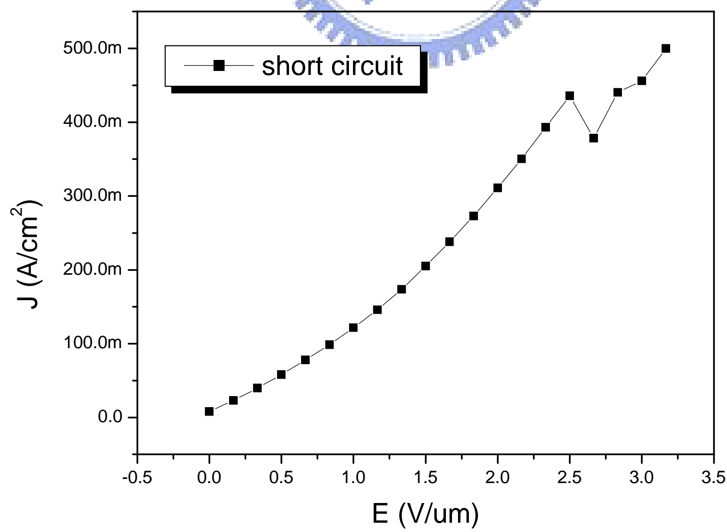

(c)

Fig. 3-2 (a) top view of conventional lateral device, (b) cross section of conventional lateral device, and (c) short circuit problem between emitters and electrode

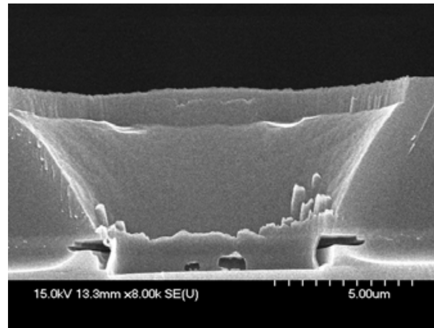

(a)

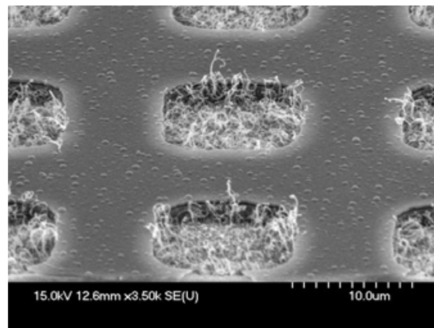

1896

(b)

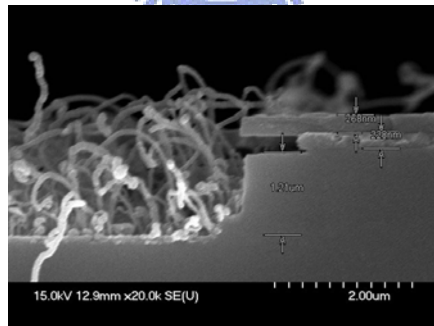

(c)

Fig. 3-3 SEM of nitride-insulted gate structure (a) the morphology before lift-off process, (b) top view and (c) cross section

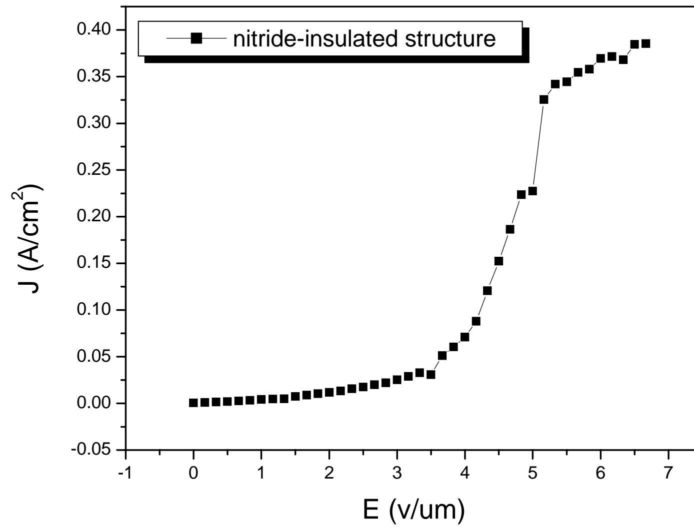

(a)

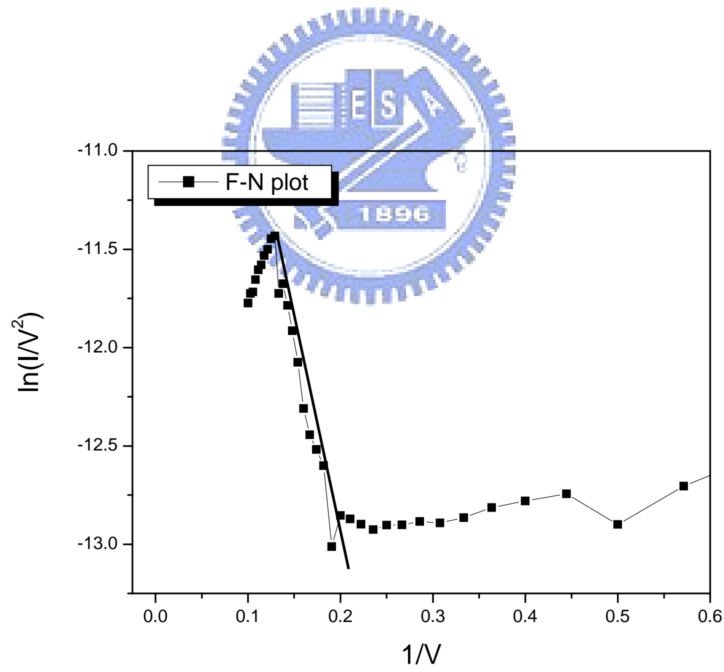

(b)

Fig. 3-4 (a) Characteristics of emission current density (J) versus applied electric field (E) for the CNTs with nitride-insulated lateral device, (b) the corresponding F-N plots.

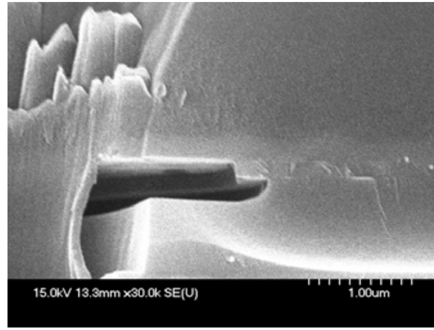

(a)

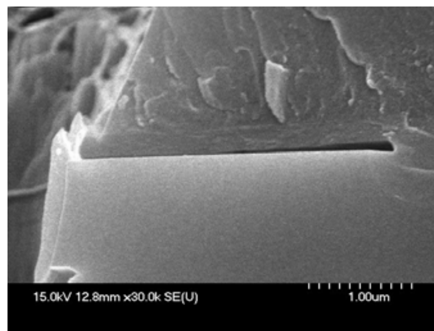

(b)

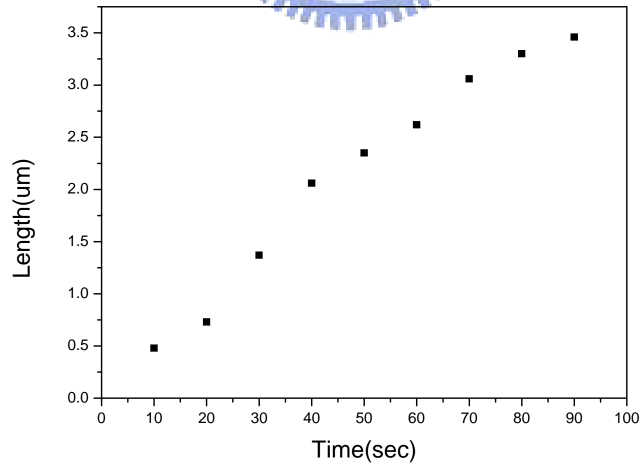

(c)

Fig. 3-5 (a)-(b) SEM of nitride-insulted gate structure with different side etching time (a) 20sec and (b) 90sec, (c) schema of the length of CNTs versus etching time

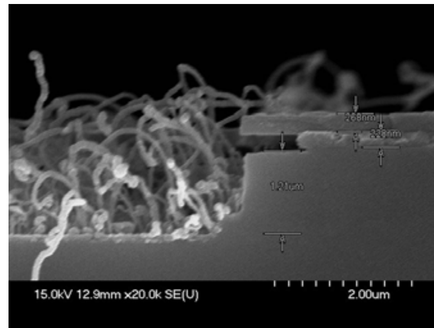

(a)

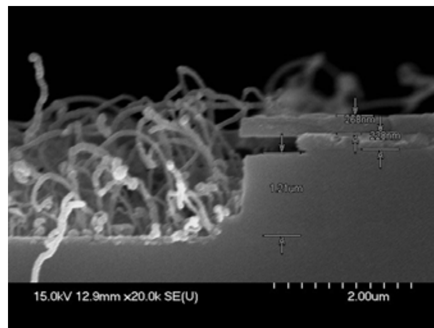

(b)

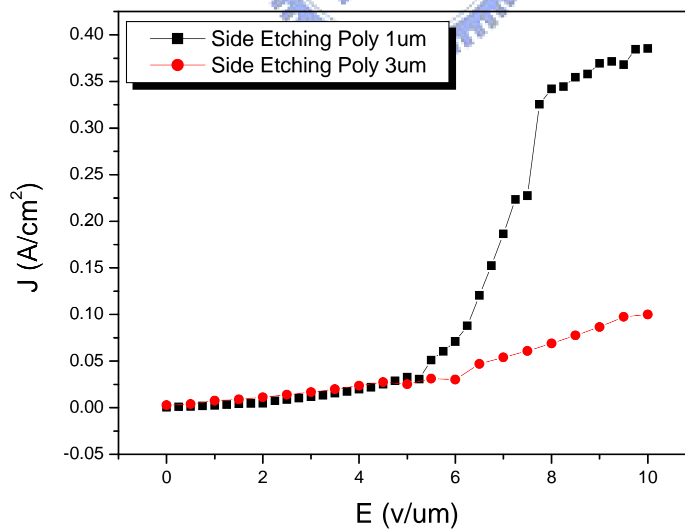

Fig. 3-6 (a)-(b) SEM of nitride-insulted gate structure with different spacer (a) 1um and (b) 3um, (c) characteristics of emission current density (J) versus applied electric field (E) for the CNTs with different spacer

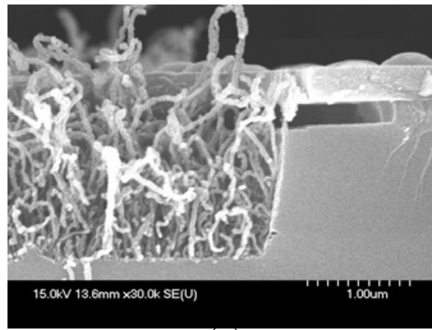

(a)

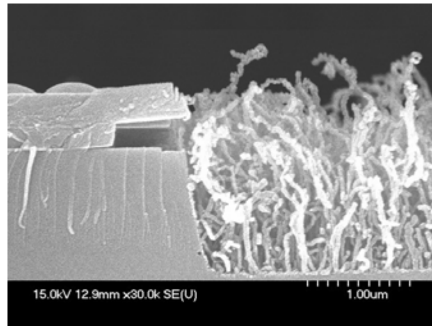

(b)

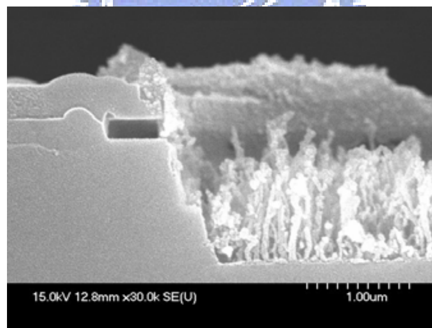

(c)

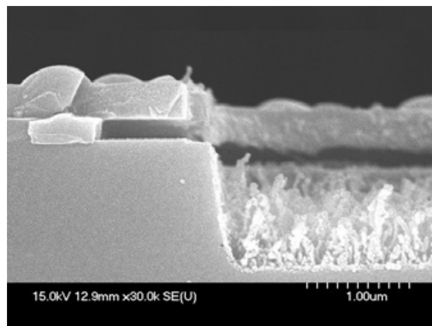

(d)

Fig. 3-7 SEM of nitride-insulted gate structure with different Ar plasma post-treatment time (a) without post-treatment (b) 15seconds, (c) 30seconds, (d) 45seconds.

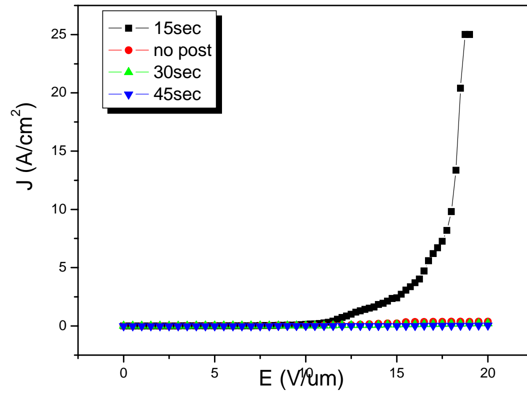

(a)

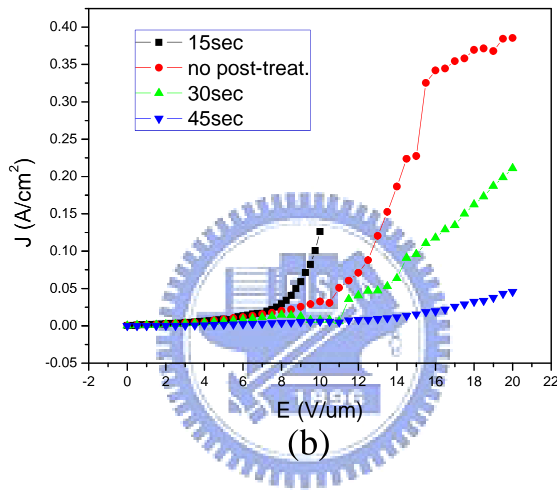

(b)

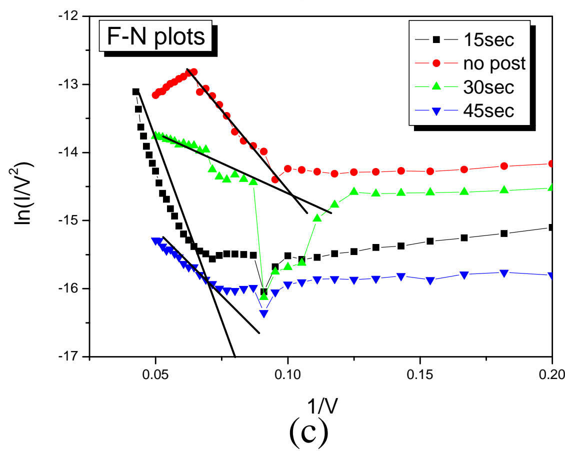

(c)

Fig. 3-8 (a) Characteristics of emission current density (J) versus applied electric field (E) for the CNTs with different plasma post-treatment time, (b) cut-off the current level with pretreatment in 15sec and can compare the turn-on field to the others, (c) the corresponding F-N plots.